Version of Record: https://www.sciencedirect.com/science/article/pii/S0266353822000355
Manuscript_d28862b4316273d6cba14efa12bc7962

A Machine Learning Approach to Determine the Elastic Properties of Printed Fiber-Reinforced Polymers

Akshay J.Thomas[a,b,*], Eduardo Barocio[b], R. Byron Pipes[a,b]

[a] *School of Aeronautics and Astronautics, Purdue University, West Lafayette, IN, 47907*
[b] *Composites Manufacturing and Simulation Center, Purdue University, West Lafayette, IN 47906*

Abstract

This work focuses on the simultaneous determination of the elastic constants and the fiber orientation state for a short fiber-reinforced polymer composite by performing a minimum of experimental tests. We introduce a methodology that enables the inverse determination of fiber orientation state and the in-situ polymer properties by performing tensile tests at the composite coupon level. We demonstrate the approach for the extrusion deposition additive manufacturing (EDAM) process to illustrate one application of the methodology, but the development is such that it can be applied to short fiber-reinforced polymer (SFRP) systems processed via other methods. Currently, developing composites additive manufacturing digital twins require extensive material characterization. In particular, the mechanical characterization of the orthotropic elastic properties of a composite involves extensive sample preparation and testing, therefore the elasticity tensor is generally populated using a micromechanics model. This, however, requires measuring the fiber orientation state in addition to knowing the constituent material properties. Experimentally measuring the fiber orientation state can be tedious and time consuming. Further, optical methods are limited to resolving the orientation of cylindrical fibers or cluster of non-cylindrical fibers, and computed tomography (CT) methods scan regions of volume that are much smaller than a full printed bead. Therefore, we propose a methodology, accelerated by machine

*Corresponding Author
Email address: `ajacobth@purdue.edu` (Akshay J.Thomas)

learning, to identify the anisotropic mechanical properties and fiber orientation state at the same time. Early results show that inference of the fiber orientation and composite properties is possible with as few as three tensile tests. Our results show that a combination of the choice of the micromechanics model and reliable set of experiments can yield the nine elastic constants, as well as, the fiber orientation state.
Keywords: Inverse Determination, Short Fiber Composites, Elastic Properties, Fiber Orientation State, Extrusion Deposition Additive Manufacturing, Support Vector Regression

1. Introduction

Short-fiber reinforced polymers (SFRP) are widely used in composite manufacturing processes such as Material Extrusion Additive Manufacturing (MEAM) and injection molding due to its easy processability. SFRP involve fibers with lengths in the range of $200 - 400\ \mu m$) [1]. Injection molded short fiber composites are utilized in lightweight applications due to short time and low cost of processing, and increased stiffness and strength [2, 3]. SFRP have also enabled scaling the MEAM process to the scale of multiple meters by decreasing the coefficient of thermal expansion and enhancing the elastic properties of the printed material, dominantly in the print direction [4]. Extrusion deposition additive manufacturing (EDAM) has lately been used to print geometries for autoclave tooling and compression molding [5, 6]. EDAM is a process by which fiber-reinforced polymer composites are melted in an extrusion system and deposited onto a bed (either moving or stationary) in a path prescribed by a machine code. The printing process involves multiple physics that develop concurrently, including anisotropic heat transfer, shrinkage, creep and stress relaxation, polymer crystallization and melting, and fusion bonding. Further, the combined effect of these phenomena lead to deformation and residual stresses that can cause issues such as delamination. This has motivated the development of physics-based [7–10] and eigenstrain-based methods [11–13] to predict the outcome of the printing process. Physics-based simulations have been used to predict and optimize the yield stress of printed acrylonitrile–butadiene–styrene(ABS)

[14]. Physics-based failure criteria for parts manufactured by selective laser sintering has been reported in [15]. The effect of printing angle angle and layer thickness on the strength and elastic properties of parts manufactured by fused deposition modeling (FDM) has been studied in [16].

To reduce the time and costly empirical calibration of processing parameters there has been much interest in developing simulation capabilities to predict the outcomes of a given print geometry or strategy [7, 9, 10]. The focus of these studies have been developing a manufacturing digital twin that can predict the deformation and residual stress state that arises from the highly non-isothermal printing conditions and material anisotropy. These manufacturing simulations require the mechanical properties of the composite as inputs to predict the deformation and residual stress state. The mechanical, transport, and thermoviscoelastic properties of the printed composite are dependent on the properties of the constituents (fiber and polymer), and the microstructural characteristics of the printed bead such as the fiber length distributions, the fiber aspect ratio, and the orientation state of the fibers. The orientation distribution of is one of the key features that govern the mechanical, transport, and thermoviscoelastic properties of the composite [17, 18]. The anisotropic mechanical properties are typically characterized via experimental methods. However, characterizing all the properties of the composite via experiments is laborious and, therefore, micromechanics models have been used to augment experimental measurements. To make use of suitable micromechanics models, the orientation and length distribution of the fibers, and the mechanical properties of its constituents are needed. The predictions from the micromechanics models and the experimental results can then serve as inputs to manufacturing digital twins for additive manufacturing.

To inform the manufacturing digital twin, simulation methods have been developed to predict the orientation of fibers in injection and compression molding [1], [19–21]. Experimental methods including CT scans and optical microscopy can be used to measure the orientation state of the fibers. However, these methods are time consuming and are prone to human error, requiring multiple iterations of the same experiment.

Furthermore, the methods for resolving fiber orientation from 2D images are limited to cylindrical fibers [22] or to clusters of non-cylindrical fibers [23]. Similarly, the spatial resolution required to resolve fiber orientation from Computed tomography (CT) scans is restricted to volumes that are often smaller than the volume of a printed bead. Another important property that governs the elastic properties of short fiber composites is the fiber length distribution [19], [20]. The initial fiber length distribution is consequently affected by fiber breakage during the manufacturing process [24], [25]. In addition to these parameters, the processability of the polymers is modified via additives which in turn can change its elastic properties.

To reduce extensive material characterization and experimental measurements required, Digimat provides a suite of 'reverse engineering' (inverse determination) capabilities to infer unmeasured properties. 'Reverse engineering' is an optimization process in which the optimal values of design variables (e.g. material law parameters) are found via minimizing the difference between model predictions and experimental measurements. The state-of-the-art in Digimat currently enables the user to inversely determine model parameters in thermo-viscoelastic material models, fiber aspect ratio, failure criterion variables, etc. This enables the user to populate the material properties to be used in composite manufacturing digital twins, once the fiber orientation state is known. Kurkin et.al calibrated a non-linear material model for SFRPs using reverse engineering [26], [27]. Landervik *et al.* used this methodology to calibrate an elastoplastic material model [28]. Digimat's inverse determination tool was also used to calibrate a pseudo-grain-based fatigue model in [29]. Despite the advancement in simulation capabilities to predict manufacturing process induced fiber orientation in injection and compression molding, equivalent models are under developed in EDAM. In addition to the dearth of simulation models, current inverse determination capabilities in literature also have been unable to account for the orientation of the fibers and the effective properties of the polymer matrix considering the effects of additives. To that end, this work addresses the latter limitation of the state-of-the-art. We introduce a methodology that enables the inverse determination of the orientation of the fibers and the modified polymer properties. This paper will study the EDAM process in particular to demonstrate the methodology, but the development is such that it can be applied to SFRP material systems processed through other manufacturing methods. We aim to extend the current capabilities of 'reverse engineering' in Digimat for the circumstance of limited experimental measurements and, with the use of a suitable micromechanics model, characterize the full mechanical SFRP composite elasticity tensor.

There are three components in the proposed inverse determination process. First, we utilize a micromechanics model to predict the composite elastic properties based on the constituent properties. Second, we conduct a limited set of experimental tests to infer the fiber orientation and polymer properties. And, third, we implement a mathematical framework that enables the inference of fiber orientation and effective polymer properties by connecting the model predictions to the experimental measurements. We discuss each of these in the following sections.

2. Micromechanics Model

First, we discuss the micromechanics model. The microstructure of a multiphase composite is typically homogenized using a Mean Field Homogenization (MFH) method to transition from the microscale constituent properties to the macroscale response of the composite. A two-step homogenization method [30] which utilizes the Mori-Tanaka model is used in this work [31]. We use the two-step homogenization method with the Mori-Tanaka/Voigt model owing to its success in predicting effective properties of two-phase composites [30, 32, 33]. The model invokes the dilute suspension assumption making it suitable for composites with low fiber volume fraction, up to approximately 25% by weight for carbon fibers. Therefore, this paper focuses on low fiber volume fraction composite materials. Nevertheless, it is important to note that the inference methodology discussed in this work can be applied to higher fiber content given the appropriate micromechanics models that represents the high fiber content system well. The micromechanics model requires a list of inputs at the microscale to make predictions at the macroscale. These include the mechanical properties of the transversely isotropic fibers, the fiber aspect ratio, fiber orientation, and constituent polymer properties (isotropic). Since we aim to inversely determine the fiber orientation and polymer properties, the other inputs are given to the model. The material system used in this study is short fiber 20 percent by weight carbon fiber (CF)- Polyetherimide (PEI) produced by SABIC (LNP™THERMOCOMP™AM COMPOUND EC004EXAR1). The transversely isotropic fiber properties of the fiber were found in the literature [34]. The fiber length distribution was measured using optical microscopy after burning off the polymer and dispersing the fibers on a glass slide as outlined in [35]. Fig. 1 shows the fiber length distribution measured experimentally . The average fiber length is divided by the average fiber diameter (measured to be 6 μm) to estimate the fiber aspect ratio. The second order orientation tensor, $\mathbb{A}$, following Advani and Tucker [36], is used to describe the orientation distribution of the fibers. The fourth-order orientation tensor is required for the orientation based stiffness averaging during the second step of the homogenization. The fourth-order orientation tensor is estimated using the second order orientation tensor using orthotropic closure approximation developed by Cintra Jr and Tucker III [37]. The orthotropic closure approximation has shown to produce acceptable results for composite stiffness predictions as shown in [33]. However, it is important to note that there are cases where the second-order fiber orientation description might prove insufficient [38]. In this study, the fibers orientation is assumed to possess only the three diagonal terms in the principal directions as done in [39]. Also, since the diagonal entries on the orientation tensor add to one, we are left with four properties that are to be inversely determined, i.e., the matrix modulus (E_m), matrix Poisson's ratio (ν_m), and the two terms of the orientation tensor (a_{11}, a_{22}). The variable a_{33} is calculated by, $a_{33} = 1 - a_{11} - a_{22}$. We present the application of our methodology for an additional material system - 25 percent by weight carbon fiber (CF) Polyethersulfone (PESU) produced by Techmer (Electrafil® PESU 1810 3DP) as a validation case in Sec. 5.3.

3. Experimental Methods

3.1. Specimen Preparation

Having discussed the micromechanics model, we now discuss the methods to prepare specimens and the experimental tensile tests conducted. Specimens to be tensile tested are prepared from panels which were printed on the Composites Additive Manufacturing Research Instrument (CAMRI). CAMRI is a medium scale extrusion deposition system developed at Purdue University to investigate the phenomenon governing the manufacturing process in EDAM. Details about of the system can be found elsewhere [40]. Three sets of specimens are required to perform the necessary tests to obtain the tensile modulus of the printed composite in the three material directions and two of the three Poisson ratios, i.e., E_1, E_2, E_3, ν_{21}, and ν_{13}. Fig. 2 shows the material orientation where the 1-direction corresponds to the printing direction, the 2-direction corresponds to the direction transverse to this direction in the printing plane, and the 3-direction corresponds to the stacking direction of the printed beads.

To prepare specimens for the tensile tests in the three material directions, panels were printed in two different orientations. A nozzle with an diameter of 4 mm was used in the CAMRI system and the bead deposition conditions were set such that the printed bead had final dimensions of 6.15 mm and 1.5 mm in width and height, respectively. The processing conditions were kept the same while printing both the panels. Fig. 2 (a) shows the panels used for preparing specimens for characterizing the elastic properties in the 1 and 3 directions. Similarly, Figure 2 (b) shows the panels used for preparing specimens for characterizing the elastic properties in the 2-direction. On the one hand, Panel A was printed with three beads across the width which produced panels with final dimensions of L=320 mm, W = 18.45 mm, H = 321 mm (Fig. 2 (a)). The two side beads in panel A were removed through a machining operation. On the other hand, panel B was printed with six beads stacked in the 3-direction which produced panels with final dimensions of L=175 mm, W = 159.9 mm, H = 9 mm (Fig. 2 (b)). The top and bottom beads in panel B were removed through a machining operation. A heat treatment at the glass transition temperature of the polymer (210° C) followed the machining process of the panels to promote relaxation of thermal residual stresses induced during the printing process. Tensile specimens were cut using a waterjet system and then dried in an oven at 100 C for one hour to remove moisture from the waterjet cutting. Once the specimens were dried, the specimens were spray painted with white matte paint and speckled to be prepared for digital image correlation (DIC) based strain measurements. The paint was left to dry for 24 hours before speckling with a black stochastic pattern. Care was taken to apply only a thin layer of paint to avoid measuring the compliance of the paint during the strain measurements.

3.2. Mechanical Testing

The tensile tests were conducted according to the ASTM D3039 standard – Standard Test Method for Tensile Properties of Polymer Matrix Composite Materials [41]. The DIC was performed using a two-camera setup (5-megapixel cameras/17 mm lenses) with the VICSnap and VIC 3D software (Correlated Solutions). The specimen was illuminated using a set of lights to improve the contrast and to focus the speckled pattern on the specimen and care was taken not to overexpose the region of interest. Hydraulic friction wedges were used to grip the ends of the specimen. The test was conducted a rate of 1 mm/min. The test setup is shown in Fig. 3. Three sets of experiments were conducted to measure the elastic modulus in the three material directions. The specimen dimensions are shown in Fig. 4. The stress was computed by dividing the force by the average area. The average strain was computed over the speckled region illustrated in Fig. 4 (74 $\times$ 13.5 mm for specimen in 1-direction and 73 $\times$ 24 mm for specimen in the 2 and 3-directions). It is known that the fiber orientation varies throughout the dimensions of the printed bead. Therefore, by averaging the strain measurements obtained from the DIC, we average the effect of the fiber orientation distribution. Since the goal of this work is populate the elasticity tensor of the composite with few experimental tests, we do not consider the effect of variation of fiber orientation throughout the specimen. We replace the variable orientation state with an “average” and uniform orientation and since the "effective" elasticity tensor is developed by averaging the properties over the bead volume, the two approximations are consistent.

Next, the elastic modulus is measured as the slope of the linear portion of the stress-strain plot taken to be from 250 to 600 micro-strain [41]. The average moduli from the three tests are obtained to be E_1= 15.42 GPa, E_2= 5.14 GPa, and E_3= 4.12 GPa. Fig. 5 shows the elastic moduli for the tested specimens in the three directions with their average values. Note that for the remainder of the paper, reference to experimental measurements implies that the average value of each specific test is used in calculations. The average Poisson's ratio was characterized as ν_{21} : 0.18 and ν_{13} : 0.35

4. Formulation of Inference Process

4.1. Background on Support Vector Regression

We now present the mathematical formulation for the inverse determination problem. Inverse problems are often found in medical imaging [42] and in areas of geophysics with application to mineral and oil exploration [43]. The inverse determination problem can be stated as :

$$\mathbf{x}^* = \underset{x}{\operatorname{argmin}}\ \mathcal{L}(f(\mathbf{x}), \mathbf{y}), \tag{1}$$

where $\mathcal{L}$ is a suitable error metric. We propose a squared error loss metric as:

$$\mathcal{L}(\mathbf{f}(\mathbf{x}), \mathbf{y}) = \sum_{i=1}^{3} \left(\frac{f_i(\mathbf{x})}{y_i} - 1 \right)^2, \tag{2}$$

where $f_i(\mathbf{x})$ is the model prediction for the corresponding experiment y_i. The model at hand is the micromechanics model discussed in section 2 and the model parameters are the matrix modulus (E_m), matrix Poisson's ratio (ν_m), and the two terms of the orientation tensor (a_{11},a_{22}). The micromechanics model predicts the nine independent elastic constants necessary to describe an orthotropic material system. However, only five of the nine elastic constants are experimentally determined, namely - E_1, E_2, E_3, ν_{21} and ν_{13}. Notice in Eq. (2) the summation is for $i = 1, 2, 3$. This has been explicitly stated since we compare the inference process under two settings. First, we consider the case where the three elastic moduli of the composite, namely E_1, E_2, and E_3, are measured experimentally. Second we consider the case where only E_1, E_3 and ν_{13} are known. The motivation behind assessing the inference problem under the second setting is to investigate if the polymer properties and the fiber orientation state could be inferred from a reduced set of experimental measurements, namely properties measured from specimens extracted from a single printed panel (Panel A, Fig. 2 (a)). Recollect that Panel A is used to measure the elastic moduli in the 1 and 3 directions. These tensile tests can be used to identify the value of ν_{13} as well. Therefore, by studying the second setting we assess the feasibility of the inference problem when only one of the two panels is printed.

Referring back to Eq. (2), we choose this loss to have normalized values across different experiments. Further, directly minimizing Eq. (2) is not computationally feasible owing to the cost of evaluating expensive micromechanics models. Therefore, the loss function $\mathcal{L}$ is replaced with a surrogate, $\mathcal{L}'$, which is computationally inexpensive to evaluate [44]. In particular, we use the support vector regression method (SVR) [45] to create a surrogate for parameter-loss pairs. This surrogate enables the use of suitable (potentially expensive) micromechanics model while keeping the inference problem computationally feasible. It is important to mention that the minimization problem can be solved using derivative free optimization methods which include the genetic algorithm, particle swarm optimization, and simulated annealing [46]. However, search algorithms may require a large number of function evaluations to reach a minima. Bayesian optimization, as used in [47], can also be used for the inference in the case of expensive micromechanics models.

SVR defines a generalized linear model as:

$$\mathcal{L}'(\mathbf{x}, \mathbf{w}, b) = \mathbf{w}^T \Phi(\mathbf{x}) + b, \tag{3}$$

where w is the weights vector for the non-linear basis functions, $\Phi(\mathbf{x})$. SVR models promote generalizability to unseen data by defining an ϵ-insensitive tube around the predictions. The parameter b accounts for biases that need to be learned from data. The learning problem is formulated as:

$$\underset{w,b,\xi,\xi^*}{\text{argmin}}\ \mathbf{w}^T\mathbf{w} + C\sum_{i=1}^{n}\xi + \xi^*, \tag{4}$$

subject to:

$$\mathcal{L}_i - (\mathbf{w}^T\Phi(\mathbf{x}) + b) \leq \epsilon + \xi_i \tag{5}$$

$$(\mathbf{w}^T\Phi(\mathbf{x}) + b) - \mathcal{L}_i \leq \epsilon + \xi_i^* \tag{6}$$

$$\xi_i, \xi_i^* \geq 0. \tag{7}$$

The index i refers to the training data. The term $\frac{1}{2}\ \mathbf{w}^T\mathbf{w}$ in Eq. (4) serves as regularization term and avoids overfitting, i.e., $\frac{1}{2}\ \mathbf{w}^T\mathbf{w}$ prevents extremely large values of w and enhances the generalizability of the regression model. The term $C\sum_{i=1}^{n}\xi + \xi^*$ is the training error term which shows the effectiveness of the regression model to learn $\mathcal{L}_i$, and C is a positive constant that determines the amount of penalized loss during the optimization process. A greater value of C promotes the algorithm to minimize the empirical risk, which is defined as the difference between the regressor prediction (i.e., the value of $\mathbf{w}^T\Phi(\mathbf{x}) + b$) and the actual value, $\mathcal{L}$. A smaller value of C allows the errors to be excessively tolerated causing the regressor predictions to be poor. ξ_i and ξ_i^* are the slack variables that specify the training error with an insensitivity region of $\pm\epsilon$. We choose the value of C using a grid search cross validation which is explained in the next section. The effect of the slack variables is enforced in Eq. (5) and Eq. (6) as constraints. The illustration shown in Fig. 6 shows the ϵ -insensitive tube in dotted lines. The data points lying inside this tube, and shown as hollow circles, are not penalized. The solid circles in Fig. 6 are outside the tube and hence have 'slack' that needs to be compensated by changing the regressor parameters (i.e. w and b).

Next, we present a crucial aspect in the learning of the SVR parameters, $\mathbf{w}$ and b, i.e., choosing the right basis transformation $\Phi(\mathbf{x})$. Choosing the right basis functions for the non-linear transformation of the inputs ($\Phi(\mathbf{x})$), is often difficult due to the lack of knowledge of the input – output relationship. SVR is trained in the dual space and requires only the evaluation of the kernel function defined by $K(\mathbf{x}_i, \mathbf{x}_j) = \langle \Phi(\mathbf{x}_i), \Phi(\mathbf{x}_j) \rangle$, where $\langle \cdot, \cdot \rangle$ represents the dot product. This investigation uses a standard radial basis kernel defined by $K(\mathbf{x}_i, \mathbf{x}_j) = \exp(-\gamma |\mathbf{x}_\mathrm{i} - \mathbf{x}_\mathrm{j}|^2)$. Further details of the theory behind SVR is explained elsewhere [45]. The choice of the radial basis kernel is supported by the fact that the radial basis kernel spans an infinite dimension and hence can approximate complex input-output relationships.

4.2. Data Set Creation and SVR training

To train the SVR, inputs were generated from a Latin Hypercube design [48] and the loss function, shown in Eq. (2), is evaluated at each of the design points to create a dataset of input-loss pairs ; $\mathcal{D} = \{\mathbf{x}_i, \mathcal{L}_i\}$. Some of the design points generated violate the physical constraint enforced by the statistical description of the orientation tensor:$a_{11} + a_{22} \leq 1$. Therefore, we discard the points from the dataset that violate this constraint. The entries of this 4-D vector are the matrix modulus (E_m), matrix Poisson's ratio (ν_m), and the two terms of the orientation tensor (a_{11},a_{22}), i.e. $\mathbf{x} = (E_m, \nu_m, a_{11}, a_{22})$. Note that the third diagonal entry of the orientation tensor, a_{33}, can be calculated by $a_{33} = 1 - a_{11} - a_{22}$. The fitting process can now be performed as outlined in the previous section. However, there are multiple parameters that need to be user-specified. First, the value of the parameter C in Eq. (4) has to be chosen. Second, we need to choose the value of the parameter, γ, to defining the radial basis kernel. Note that the parameters C and γ are dependent and hence it becomes difficult to manually find the right combination that produces the best regressor prediction. To that end, we use the Grid Search Cross-Validation [49] method to find the best combination of these parameters. Grid search is a method by which the range and step size of all the parameters are specified and each combination of the hyperparameter set is tested to find the best one via a k-fold cross validation. In the k-fold cross validation, the data is divided into k groups after which $k-1$ groups are used for the training process and the remaining one group is used as a test data set. This is done k times until each group acts as test data set at least once. The average of the test error score serves as a measure of the effectiveness of a particular combination of parameters in explaining the data. Once the k-fold cross validation is conducted for each hyperparameter combination, the set with the least test error is chosen as the optimal parameter set. It is important to note here that grid-search is an expensive approach and cannot be used in cases with large number of parameters to be tuned. There are other methods for parameter tuning including Bayesian optimization [50] and metaheuristic algorithms such as particle swarm optimization, ant colony optimization, and genetic algorithms [51–53]. We choose the grid search method owing to its ease in implementation and understanding. In this study we choose k=5, i.e., we use a 5-fold cross validation for the parameter tuning. To evaluate the regressor performance on the test set the R^2 score is used. To clarify, the average R^2 value obtained from the k folds is reported as the test score.

4.3. Inference Process

Once the SVR surrogate is trained, the inference of the fiber orientation and the polymer elastic properties can be performed. The inference problem can be solved by minimizing the response of the SVR surrogate, i.e., the minimization problem in Eq. (1) is restated as:

$$\mathbf{x}^* = \underset{x}{\operatorname{argmin}}\ \mathcal{L}'(\mathbf{x}, \mathbf{w}, \mathbf{b}). \tag{8}$$

Since we found the values $\mathbf{w}$ and $\mathbf{b}$ during the training process, Eq. (8) represents an optimization problem in only $\mathbf{x}$. In this study the sequential linear least squares quadratic programming (SLSQP) is used owing to its flexibility to handle constraints and bounds [54]. Note that there are no equality or inequality constraints in our inference problem, however, the parameters to be inferred are bounded. The bounds chosen are given in table 1. Bounds are chosen based on the material being printed and the system used to print it. For example, from previous printing experience [39], we anticipate the value of a_{11} to be greater than 0.45 and therefore it is kept as a lower bound. The code for the SVR surrogate training and the optimization is implemented in Python using open source packages [55]. The inference process is illustrated using a flowchart shown in Fig. 7.

5. Results and Discussion

5.1. Inference using E_1, E_2 and E_3

We first present the results for the case where we use the three experimentally measured composite elastic moduli, ie., E_1, E_2 and E_3 for the inference process. A dataset D of size 202 points is created for the training process. Here, the 202 data points are created after rejecting the points which vioaltes the constraint of $a_{11} + a_{22} \leq 1$. Next, the SVR surrogate is trained using the Grid-Search cross validation to find the best combination of hyperparameters. The range of the parameter, C is chosen to be 15 equally spaced values between 1 and 100. For the parameter γ, 20 equally spaced values between 1 and 20 are chosen. The value of ϵ is chosen to be 0.05, i.e. during the training process for the loss surrogate the prediction errors below 0.05 are not penalized. The best hyperparameter obtained is the combination of C= 100.00 and γ=5.00. The R^2 value obtained for the best hyperparameter setting is 0.993 indicating that the predictor represents the data well within the bounds of the ϵ-insensitive tube. In this case we notice that the parameter C attains the largest value in the grid search. However, it is noticed that further increasing the upper bound of C does not change the prediction of the regressor. Now, we conduct the optimization as stated in Eq. (8) using the SLSQP method. Since the SLSQP method is a gradient based method the optimization step is conducted with different starting points to evaluate the possibility of local convergence. It was observed that different starting points converged to the same optimal value. Further, to confirm the minimum obtained is indeed a global minimum the dual annealing global search [56] is used to search for the minimum. It was found that all the former runs yield the same result indicating that the minimum obtained from SLSQP is indeed the global minimum. The inversely determined properties are summarized in table 2.

We now use these inferred values as inputs to the micromechanics model to predict the composite level mechanical properties and compare them to the experimentally observed values. To serve as a test case of the proposed method, we measure the shear modulus in the 1-3 direction by preparing samples from Panel A. The shear modulus was characterized according to the D5379 Standard Test Method for Shear Properties of Composite Materials by the V-Notched Beam Method [57]. Table 3 shows that the composite stiffness predictions using the inferred properties are in good agreement with the mean experimental values. First, we see that the three elastic moduli are in good agreement with predictions. This is expected since the average elastic moduli were used in the inference process. Second, we also see that the values of ν_{13} almost match exactly. Third, it is important to note that the values of the shear modulus, G_{13}, do not match exactly. This could be attributed to the fact that the micromechanics model neither accounts for the variation of orientation of the fibers within a printed bead nor for the effect of the interface developed between adjacent layers.

The effect of this variation could be pronounced under shear loading leading to different shear modulus predictions from the micromechanics model. Further, it should be noted that the fiber properties were taken [34] which might not represent the actual fiber properties used in this SFRP system. The discrepancy in the ν_{21} could also be affected by the fact that signal-to-noise ratio is low when measuring small strains via the DIC. To clarify, the strain in the 1-direction (printing direction) is low due to the preferential alignment of fibers in this direction during the printing process. This could lead to erroneous experimental measurements and thereby augment the prediction error.

5.2. Inference using E_1, E_3 and ν_{13}

We now present the results for the case where we use E_1, E_3, and ν_{13} for the inference process. Similar to the previous section we create a dataset of 202 points which is a result of rejecting the data points that violate the constraint of $a_{11} + a_{22} \leq 1$.

Again, the SVR surrogate is trained using the Grid-Search cross validation to find the best combination of hyperparameters and the value of ϵ is kept to be 0.05. The best hyperparameter combination obtained in this case is again $C = 100.00$ and $\gamma = 5.00$. The R^2 value obtained is 0.994 indicating that the predictor represents the data well within the bounds of the $\epsilon-$insensitive tube. Next we perform the optimization to infer the polymer properties and fiber orientation state. The inferred properties are listed in table 4. Comparing the inferred results in table 4 we see that they match closely with the values in table 2. The components of the orientation tensor (a_{11} and a_{22}) in table 4 match exactly with the values in table 2. There is a slight variation in the inferred matrix properties which is the result of differences in the loss function when we use different set of experimental values. Nonetheless, this result clearly indicates that we can infer the effective polymer properties and fiber orientation state by printing only Panel A. This observation is important since this can significantly reduce the experimental efforts of material characterization. However, to completely validate the claim of needing to print only one panel, we need to apply this methodology to a different material system and therefore it will be a topic of future investigations.

We now use these inferred values as inputs to the micromechanics model to predict the composite level mechanical properties and compare them to the experimentally observed values. This is shown in table 5. We find that overall the results are in good agreement with the experimental values. We notice again the error is pronounced in the G_{13} and ν_{21} predictions. This is anticipated since the inferred values in this case are similar to the case presented earlier. These results indicate the potential of our methodology in reducing experimental characterization efforts considerably.

5.3. Inference results for CF-PESU

We present the results of our outlined methodology applied to an additional material system - 25 percent by weight CF-PESU. Following the same method as outlined earlier, we create a data set of size 202 points for the training procedure. The range of the parameter, C, is chosen to be 15 equally spaced points between 1 and 100. For the parameter, γ, 20 equally spaced values between 1 and 15 is chosen. The experimental data for the inference is taken from [58]. We use the stiffness values - E_1, E_2, and E_3 for the inference. The inversely determined properties are summarized in table 6. Using the inferred values as inputs to the micromechanics model, we predict the composite level mechanical properties and compare them to the experimental values obtained from [58]. This is shown in table 7. Notice that eight out of the nine independent constants have been experimentally measured by Ramirez [58] and therefore serves as a good validation case for our methodology.

From table 7 we see that the predictions for E_1, E_2, and E_3 are in good agreement with the experimental measurements. This is expected since we used these values for the inference. In this case, we also notice that ν_{21} prediction is in better agreement with the experimental value compared to the case with CF-PEI discussed earlier. Further, the ν_{13} values match exactly. We also see that the predictions of G_{12} and G_{23} are in good agreement with the experimental values. However, the error in the G_{13} is considerable. The coefficient of variation for measuring G_{13} was calculated to be 39.45% indicating that the mean experimental value could be biased and therefore aggravate the prediction error. These results indicate that our method can be used to populate the elasticity tensor for printed short fiber-reinforced polymers and thereby is of immense importance in reducing extensive experimental characterization.

6. Conclusions

In this paper we present a methodology to infer the orientation state of the fibers and the polymer properties in a SFRP composite. This study was motivated by the need to reduce extensive experimental efforts to measure the fiber orientation and effective polymer properties. The methods implemented in this work show that we are able to infer composite properties in SFRP composites with as few as three tensile tests. The predictions of the composite elastic properties using the inferred constituent properties and fiber orientation tensor are in good agreement with the experimental measurements. There are some discrepancies in the shear modulus and the Poisson's ratio predictions.

The error in the shear modulus predictions could be attributed to the fact that the micromechanics model used in this study does not account for the variation of the fiber orientation within a bead nor for the effect of the interface of printed beads. This warrants further investigation in the form of formulating a better micromechanics model that better predicts shear behavior of the printed bead. The discrepancy in the ν_{21} predictions could be aggravated by the fact that signal-to-noise ratio is low when measuring small strains via the DIC. To clarify, the strain in the 1-direction (printing direction) is low due to the preferential alignment of fibers in this direction during the printing process. This could lead to erroneous experimental measurements and thereby augmenting the prediction error. We also identify future directions for this work in light of some limitations. The support vector regression method used requires user specification of the value of ϵ to define the ϵ- insensitive tube. We specify this value to be 0.05. However, this might not be the optimal case for other material systems or cases where the strain is measured using strain gauges. Therefore, following a Bayesian approach for the inference could make the process more robust and enable the user to calibrate both parameter and measurement uncertainty.

In conclusion, we present a method to infer the fiber orientation in a printed short fiber-reinforced composite and identify the elasticity tensor using as few as three tensile tests. Hence, this paper advances the state of the art in inverse determination beyond the available tools in Digimat and existing published literature. The potential of our method to populate the elasticity tensor just by printing one panel is of immense importance in accelerating the design phase of printed SFRP composites.

CRediT author contribution statement

Akshay J. Thomas: Conceptualization, Methodology, Software, Investigation, Formal analysis, Writing - original draft. **Eduardo Barocio**: Conceptualization, Investigation, Writing - review and editing. **R. Byron Pipes**: Funding acquisition, Supervision, Resources, Writing - review and editing.

Declaration of competing interest

The authors declare no competing financial or personal interests that could have appeared to influence this work.

Acknowledgements

This research was sponsored by the U.S. Department of Energy, Institute for Advanced Composites Manufacturing Innovation (IACMI), under contract DOE DE-EE0006926, IACMI PA16-0349-3.12-01.

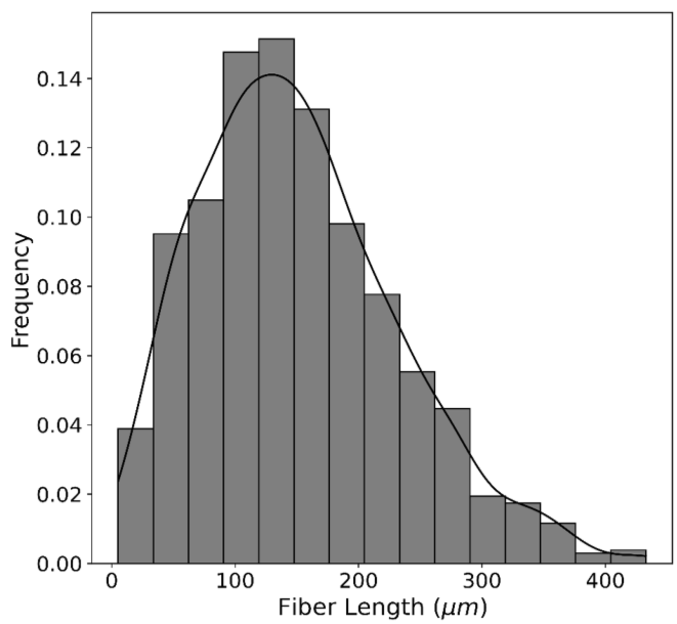

Figure 1: Fiber length distribution of the processed 20 percent by weight CF-PEI.

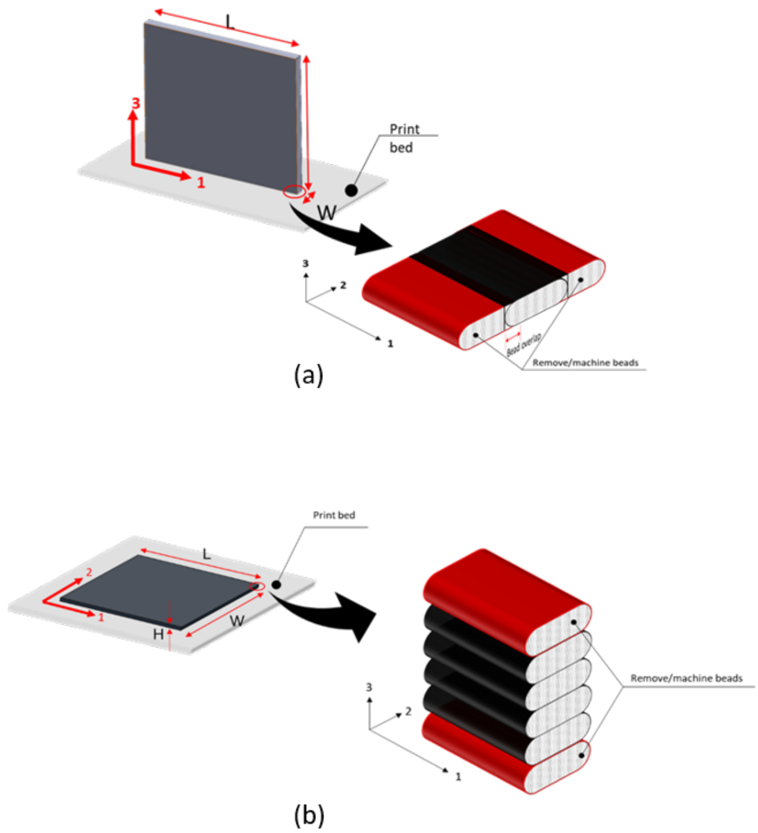

Figure 2: Illustration of (a) Panel A and (b) Panel B used to prepare tensile specimens. Note that the beads highlighted in red are machined away.

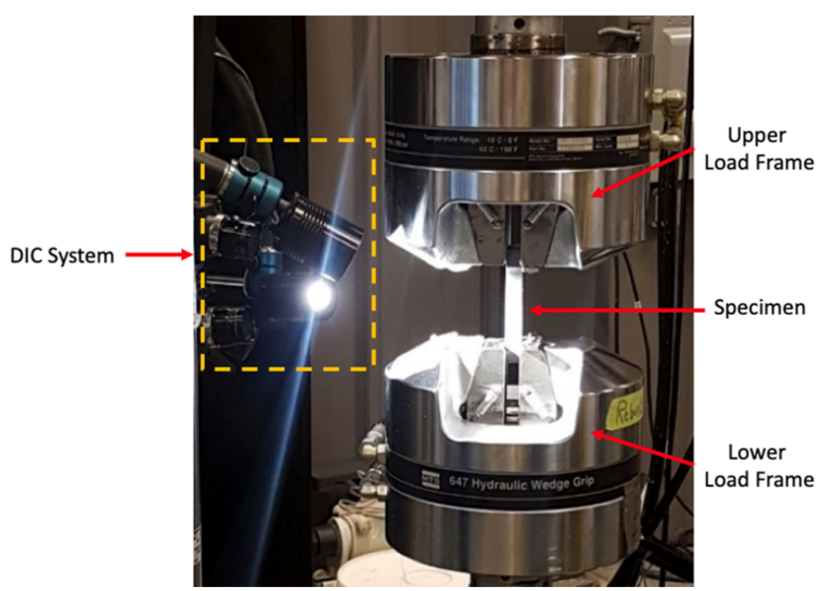

Figure 3: Experimental setup for the tensile tests.

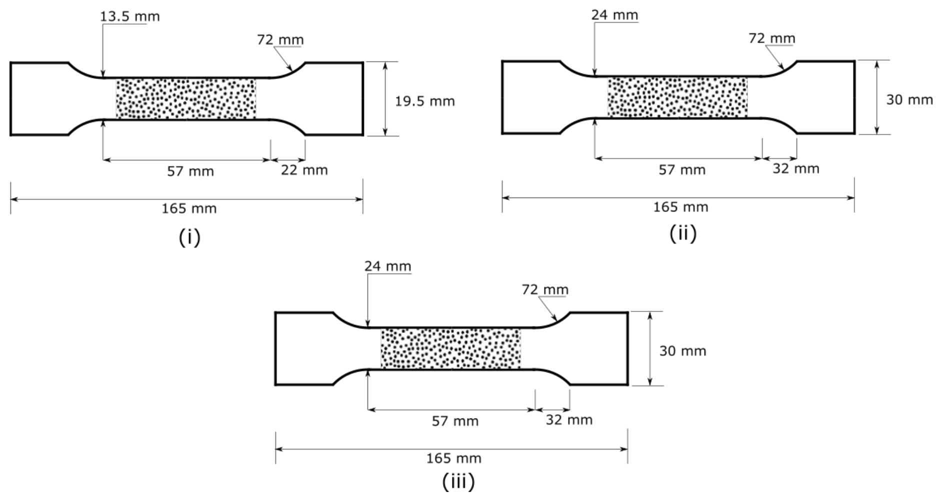

Figure 4: Specimen dimension for the tensile coupon in (i) 1-direction (printing direction) (ii) 2 -direction (transverse to printing direction) (iii) 3 -direction (stacking direction). The surface strain measured by the DIC is averaged over speckled area shown in this illustration

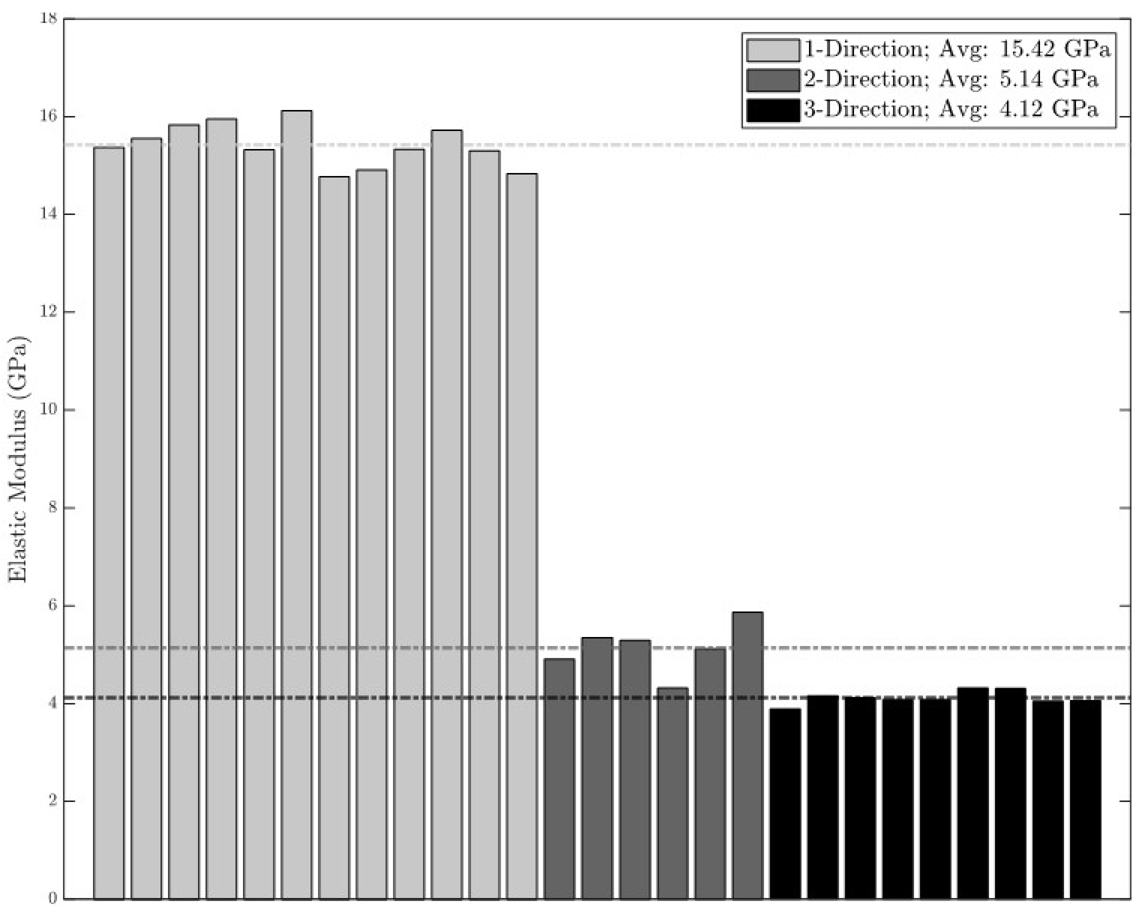

Figure 5: Experimental measurement of elastic modulus in the 1-direction, 2-direction , and 3–direction

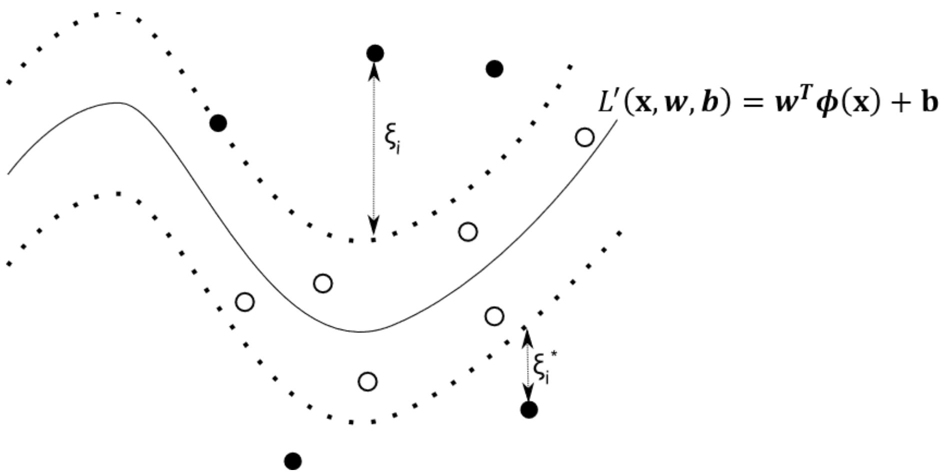

Figure 6: Non-linear SVR with the ϵ-insensitive loss tube (dotted lines)

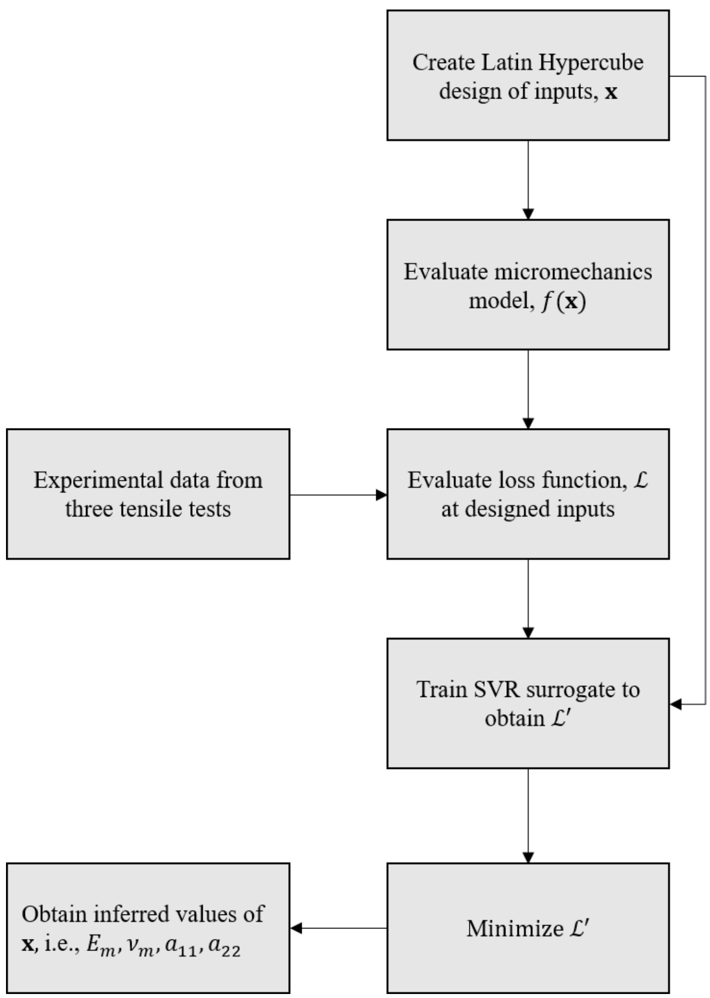

Figure 7: Flowchart illustrating the inference process

Table 1: Bounds on the parameters to be inferred

Parameter	Lower Bound	Upper Bound
Matrix Modulus, $E(GPa)$	1.50	4.20
Matrix Poisson's Ratio, ν	0.30	0.42
a_{11}	0.45	0.90
a_{22}	0.00	0.50

Table 2: Inferred properties using E_1, E_2 and E_3 for CF-PEI

Parameter	Inferred Values
Matrix Modulus, $E(GPa)$	2.72
Matrix Poisson's Ratio ν	0.36
a_{11}	0.75
a_{22}	0.17
$a_{33} = 1 - a_{22} - a_{11}$	0.08

Table 3: Composite property predictions for CF-PEI using the inferred material properties in table 2

Property	Predictions Using Inferred Properties	Mean Experimental Measurements	Percentage Error(%)
$E_1(GPa)$	14.66	15.42	4.90
$E_2(GPa)$	4.93	5.14	4.08
$E_3(GPa)$	4.22	4.12	2.42
$G_{12}(GPa)$	2.52	Not Measured	NA
$G_{13}(GPa)$	1.88	2.55	26.27
$G_{23}(GPa)$	1.53	Not Measured	NA
ν_{21}	0.14	0.18	22.22
ν_{13}	0.36	0.35	2.78
ν_{23}	0.45	Not Measured	NA

Table 4: Inferred properties using E_1, E_3 and ν_{13} for CF-PEI

Parameter	Inferred Values
Matrix Modulus, $E(GPa)$	2.67
Matrix Poisson's Ratio ν	0.35
a_{11}	0.75
a_{22}	0.17
$a_{33} = 1 - a_{22} - a_{11}$	0.08

Table 5: Composite property predictions for CF-PEI using the inferred material properties in table 4

Property	Predictions Using Inferred Properties	Mean Experimental Measurements	Percentage Error(%)
$E_1(GPa)$	14.56	15.42	5.57
$E_2(GPa)$	4.89	5.14	4.86
$E_3(GPa)$	4.10	4.12	0.49
$G_{12}(GPa)$	2.50	Not Measured	NA
$G_{13}(GPa)$	1.86	2.55	27.05
$G_{23}(GPa)$	1.52	Not Measured	NA
ν_{21}	0.14	0.18	22.22
ν_{13}	0.35	0.35	0.00
ν_{23}	0.44	Not Measured	NA

Table 6: Inferred properties using E_1, E_2, and E_3 for CF-PESU

Parameter	Inferred Values
Matrix Modulus, $E(GPa)$	2.34
Matrix Poisson's Ratio ν	0.34
a_{11}	0.77
a_{22}	0.16
$a_{33} = 1 - a_{22} - a_{11}$	0.07

Table 7: Composite property predictions using the inferred material properties for CF-PESU

Property	Predictions Using Inferred Properties	Mean Experimental Measurements	Percentage Error(%)
$E_1(GPa)$	15.93	16.92	5.85
$E_2(GPa)$	4.73	4.85	2.47
$E_3(GPa)$	3.86	3.79	1.84
$G_{12}(GPa)$	2.54	2.88	11.81
$G_{13}(GPa)$	1.78	1.26	41.26
$G_{23}(GPa)$	1.44	1.33	8.27
ν_{21}	0.12	0.14	14.29
ν_{13}	0.34	0.34	0.00
ν_{23}	0.43	Not Measured	NA

[1] H.-C. Tseng, R.-Y. Chang, C.-H. Hsu, Numerical prediction of fiber orientation and mechanical performance for short/long glass and carbon fiber-reinforced composites, Composites Science and Technology 144 (2017) 51–56.

[2] S. Yashiro, T. Okabe, K. Matsushima, A numerical approach for injection molding of short-fiber-reinforced plastics using a particle method, Advanced Composite Materials 20 (2011) 503–517.

[3] S. Yashiro, H. Sasaki, Y. Sakaida, Particle simulation for predicting fiber motion in injection molding of short-fiber-reinforced composites, Composites Part A: Applied Science and Manufacturing 43 (2012) 1754–1764.

[4] L. J. Love, V. Kunc, O. Rios, C. E. Duty, A. M. Elliott, B. K. Post, R. J. Smith, C. A. Blue, The importance of carbon fiber to polymer additive manufacturing, Journal of Materials Research 29 (2014) 1893–1898.

[5] E. Barocio, B. Brenken, A. Favaloro, R. Pipes, Extrusion deposition additive manufacturing of composite molds for high-temperature applications, in: Proceedings of the Int. SAMPE Tech. Conf., Seattle, WA, USA, pp. 22–25.

[6] A. A. Hassen, R. Springfield, J. Lindahl, B. Post, L. Love, C. Duty, U. Vaidya, R. B. Pipes, V. Kunc, The durability of large-scale additive manufacturing composite molds, CAMX 2016 (2016) 26–29.

[7] B. Brenken, E. Barocio, A. Favaloro, V. Kunc, R. B. Pipes, Development and validation of extrusion deposition additive manufacturing process simulations, Additive Manufacturing 25 (2019) 218–226.

[8] E. Barocio, B. Brenken, A. Favaloro, M. Bogdanor, R. B. Pipes, Extrusion Deposition Additive Manufacturing with Fiber-Reinforced Thermoplastic Polymers, in: K. Friedrich, R. Walter (Eds.), Structure and Properties of Additive Manufactured Polymer Components, Woodhead Publishing, 1 edition, 2020, p. 450.

[9] P. Hébert, S. Mathieu, L. Adam, D. Gianotta, C. Basire, Holistic multiscale simulation approach for additive layer manufacturing of plastics, in: SPE ACCE Conf., pp. 1–15.

[10] M. Talagani, S. DorMohammadi, R. Dutton, C. Godines, H. Baid, F. Abdi, V. Kunc, B. Compton, S. Simunovic, C. Duty, et al., Numerical simulation of big area additive manufacturing (3d printing) of a full size car, SAMPE journal 51 (2015) 27–36.

[11] X. Liang, L. Cheng, Q. Chen, Q. Yang, A. C. To, A modified method for estimating inherent strains from detailed process simulation for fast residual distortion prediction of single-walled structures fabricated by directed energy deposition, Additive Manufacturing 23 (2018) 471–486.

[12] N. Keller, V. Ploshikhin, New method for fast predictions of residual stress and distortion of am parts, in: Solid freeform fabrication symposium, volume 25.

[13] S. Afazov, W. A. Denmark, B. L. Toralles, A. Holloway, A. Yaghi, Distortion prediction and compensation in selective laser melting, Additive Manufacturing 17 (2017) 15–22.

[14] C. Camposeco-Negrete, P.-Y. Lavertu, J. Lopez-de Alda, Prediction and optimization of the yield stress of material extrusion specimens made of abs, using numerical simulation and experimental tests, The International Journal of Advanced Manufacturing Technology (2021) 1–15.

[15] P. Obst, M. Launhardt, D. Drummer, P. Osswald, T. Osswald, Failure criterion for pa12 sls additive manufactured parts, Additive Manufacturing 21 (2018) 619–627.

[16] Y. Zhao, Y. Chen, Y. Zhou, Novel mechanical models of tensile strength and elastic property of fdm am pla materials: Experimental and theoretical analyses, Materials & Design 181 (2019) 108089.

[17] S. Mortazavian, A. Fatemi, Effects of fiber orientation and anisotropy on tensile strength and elastic modulus of short fiber reinforced polymer composites, Composites part B: engineering 72 (2015) 116–129.

[18] W. Ogierman, G. Kokot, A study on fiber orientation influence on the mechanical response of a short fiber composite structure, Acta Mechanica 227 (2016) 173–183.

[19] S. G. Advani, Prediction of fiber orientation during processing of short fiber composites, Ph.D. thesis, University of Illinois at Urbana-Champaign, 1987.

[20] M. Gupta, K. Wang, Fiber orientation and mechanical properties of short-fiber-reinforced injection-molded composites: Simulated and experimental results, Polymer Composites 14 (1993) 367–382.

[21] J. Ko, J. R. Youn, Prediction of fiber orientation in the thickness plane during flow molding of short fiber composites, Polymer composites 16 (1995) 114–124.

[22] R. S. Bay, C. L. Tucker III, Stereological measurement and error estimates for three-dimensional fiber orientation, Polymer Engineering & Science 32 (1992) 240–253.

[23] N. D. Sharp, J. E. Goodsell, A. J. Favaloro, Measuring fiber orientation of elliptical fibers from optical microscopy, Journal of Composites Science 3 (2019) 23.

[24] S.-Y. Fu, B. Lauke, Effects of fiber length and fiber orientation distributions on the tensile strength of short-fiber-reinforced polymers, Composites Science and Technology 56 (1996) 1179–1190.

[25] S.-Y. Fu, B. Lauke, E. Mäder, C.-Y. Yue, X. Hu, Tensile properties of short-glass-fiber-and short-carbon-fiber-reinforced polypropylene composites, Composites Part A: Applied Science and Manufacturing 31 (2000) 1117–1125.

[26] E. Kurkin, M. Spirina, Y. V. Zakhvatkin, V. Chertykovtseva, The influence of the weld line location on the mechanical characteristics of lugs from short fibers reinforced composite material, in: IOP Conference Series: Materials Science and Engineering, volume 868, IOP Publishing, p. 012028.

[27] E. Kurkin, M. Spirina, V. Chertykovtseva, Y. V. Zakhvatkin, Mechanical characteristics of short fiber composite samples located behind circle, rectangle, triangle obstacles, in: IOP Conference Series: Materials Science and Engineering, volume 868, IOP Publishing, p. 012024.

[28] M. Landervik, J. Jergeus, Digimat material model for short fiber reinforced plastics at volvo car corporation, in: European LS-DYNA Conference, pp. 1–9.

[29] J.-A. Lindhult, M. Ljungberg, Fatigue analysis of anisotropic short fibre reinforced polymers-by use of Digimat and nCode DesignLife, Master's thesis, 2015.

[30] I. Doghri, L. Tinel, Micromechanical modeling and computation of elasto-plastic materials reinforced with distributed-orientation fibers, International Journal of Plasticity 21 (2005) 1919–1940.

[31] T. Mori, K. Tanaka, Average stress in matrix and average elastic energy of materials with misfitting inclusions, Acta metallurgica 21 (1973) 571–574.

[32] O. Pierard, C. Friebel, I. Doghri, Mean-field homogenization of multi-phase thermo-elastic composites: a general framework and its validation, Composites Science and Technology 64 (2004) 1587–1603.

[33] D. Dray, P. Gilormini, G. Régnier, Comparison of several closure approximations for evaluating the thermoelastic properties of an injection molded short-fiber composite, Composites Science and Technology 67 (2007) 1601–1610.

[34] T. King, D. Blackketter, D. Walrath, D. Adams, Micromechanics prediction of the shear strength of carbon fiber/epoxy matrix composites: the influence of the matrix and interface strengths, Journal of Composite Materials 26 (1992) 558–573.

[35] M. A. Ramirez, In-silico Tensile Testing of Additively Manufactured Short Fiber Composite, Ph.D. thesis, Purdue University, 2018.

[36] S. G. Advani, C. L. Tucker III, The use of tensors to describe and predict fiber orientation in short fiber composites, Journal of rheology 31 (1987) 751–784.

[37] J. S. Cintra Jr, C. L. Tucker III, Orthotropic closure approximations for flow-induced fiber orientation, Journal of Rheology 39 (1995) 1095–1122.

[38] V. Müller, T. Böhlke, Prediction of effective elastic properties of fiber reinforced composites using fiber orientation tensors, Composites Science and Technology 130 (2016) 36–45.

[39] B. Brenken, Extrusion Deposition Additive Manufacturing of Fiber Reinforced Semi-Crystalline Polymers, Ph.D. thesis, Purdue University, 2017.

[40] E. B. Vaca, Fusion bonding of fiber reinforced semi-crystalline polymers in extrusion deposition additive manufacturing, School of Materials Engineering, Purdue University West Lafayette, Indiana, USA (2018).

[41] A. C. D.-. on Composite Materials, Standard test method for tensile properties of polymer matrix composite materials, ASTM international, 2008.

[42] S. R. Arridge, Optical tomography in medical imaging, Inverse problems 15 (1999) R41.

[43] W. Menke, Geophysical data analysis: Discrete inverse theory, Academic press, 2018.

[44] R. F. Gunst, Response surface methodology: process and product optimization using designed experiments, 1996.

[45] P.-S. Yu, S.-T. Chen, I.-F. Chang, Support vector regression for real-time flood stage forecasting, Journal of hydrology 328 (2006) 704–716.

[46] L. M. Rios, N. V. Sahinidis, Derivative-free optimization: a review of algorithms and comparison of software implementations, Journal of Global Optimization 56 (2013) 1247–1293.

[47] T. Chuaqui, A. Rhead, R. Butler, C. Scarth, A data-driven bayesian optimisation framework for the design and stacking sequence selection of increased notched strength laminates, Composites Part B: Engineering 226 (2021) 109347.

[48] H. Moon, A. Dean, T. Santner, Algorithms for generating maximin orthogonal and latin hypercube designs, J. Stat. Theory Pract 5 (2011) 81–98.

[49] P. Lameski, E. Zdravevski, R. Mingov, A. Kulakov, Svm parameter tuning with grid search and its impact on reduction of model over-fitting, in: Rough sets, fuzzy sets, data mining, and granular computing, Springer, 2015, pp. 464–474.

[50] A. H. Victoria, G. Maragatham, Automatic tuning of hyperparameters using bayesian optimization, Evolving Systems 12 (2021) 217–223.

[51] C. Sudheer, R. Maheswaran, B. K. Panigrahi, S. Mathur, A hybrid svm-pso model for forecasting monthly streamflow, Neural Computing and Applications 24 (2014) 1381–1389.

[52] V. N. Vapnik, An overview of statistical learning theory, IEEE transactions on neural networks 10 (1999) 988–999.

[53] D. Lixing, L. Jinhu, L. Xuemei, L. Lanlan, Support vector regression and ant colony optimization for hvac cooling load prediction, in: 2010 International Symposium on Computer, Communication, Control and Automation (3CA), volume 1, IEEE, pp. 537–541.

[54] P. E. Gill, E. Wong, Sequential quadratic programming methods, in: Mixed integer nonlinear programming, Springer, 2012, pp. 147–224.

[55] F. Pedregosa, G. Varoquaux, A. Gramfort, V. Michel, B. Thirion, O. Grisel, M. Blondel, P. Prettenhofer, R. Weiss, V. Dubourg, J. Vanderplas, A. Passos, D. Cournapeau, M. Brucher, M. Perrot, E. Duchesnay, Scikit-learn: Machine learning in Python, Journal of Machine Learning Research 12 (2011) 2825–2830.

[56] Y. Xiang, D. Sun, W. Fan, X. Gong, Generalized simulated annealing algorithm and its application to the thomson model, Physics Letters A 233 (1997) 216–220.

[57] D. ASTM, 5379/d 5379m: standard test method for shear properties of composites materials by the v-notched beam method, ASTM International, West Conshohocken, PA (2005).

[58] M. Ramirez, Computational viscoelastic damage modeling of composite materials in extrusion deposition additive manufacturing, 2021.

Credit Author Statement

Akshay J. Thomas: Conceptualization, Methodology, Software, Investigation, Formal analysis, Writing - original draft

Eduardo Barocio: Conceptualization, Investigation, Writing - review and editing.

R. Byron Pipes: Funding acquisition, Supervision, Resources, Writing - review and editing

Declaration of interests

☒The authors declare that they have no known competing financial interests or personal relationships that could have appeared to influence the work reported in this paper.

☐The authors declare the following financial interests/personal relationships which may be considered as potential competing interests:

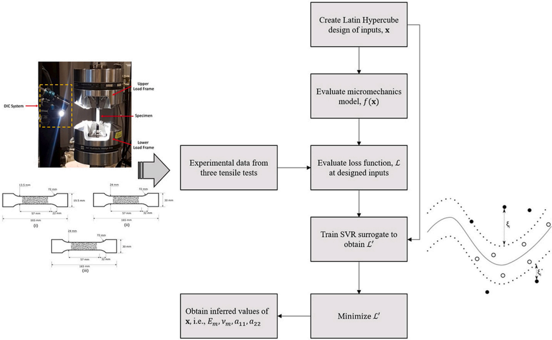
DIC System
Upper Load Frame
Specimen
Lower Load Frame
13.5 mm
72 mm
19.5 mm
57 mm
22 mm
165 mm
(i)
24 mm
72 mm
30 mm
57 mm
32 mm
165 mm
(ii)
24 mm
72 mm
30 mm
57 mm
32 mm
165 mm
(iii)
Create Latin Hypercube design of inputs, $\mathbf{x}$
Evaluate micromechanics model, $f(\mathbf{x})$
Experimental data from three tensile tests
Evaluate loss function, $\mathcal{L}$ at designed inputs
Train SVR surrogate to obtain $\mathcal{L}'$
Minimize $\mathcal{L}'$
Obtain inferred values of $\mathbf{x}$, i.e., $E_m, \nu_m, a_{11}, a_{22}$
ξ_i
ξ_i^*